Report

Current Biology

A Positive Feedback between Growth and Polarity Provides Directional Persistency and Flexibility to the Process of Tip Growth

Graphical Abstract

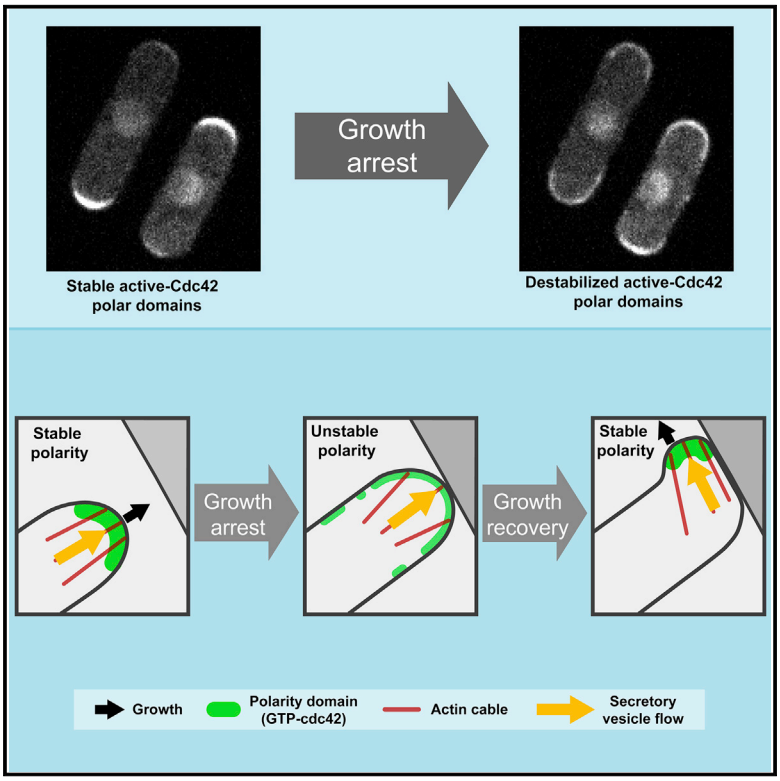

Authors

Armin Haupt, Dmitry Ershov, Nicolas Minc

Correspondence

nicolas.minc@ijm.fr

In Brief

Stable polar domains of the active form of a Rho GTPase, such as Cdc42, drive tip growth. Haupt et al. report that growth arrest destabilizes active Cdc42 polar domains, causing them to move across the cell surface. This interplay between growth and polarity allows fungal cells to redirect growth with respect to their mechanical environment.

Highlights

- Tip growth is associated with stable polarity zones enriched in active Cdc42
- Arresting growth by chemical or mechanical means destabilizes active Cdc42 domains
- The influence of growth on polarity implicates actin-based transport
- This process is relevant to the polar growth of many distant fungal species

Haupt et al., 2018, Current Biology *28*, 3342–3351
October 22, 2018
https://doi.org/10.1016/j.cub.2018.09.022

CellPress

CellPress

Current Biology
Report

A Positive Feedback between Growth and Polarity Provides Directional Persistency and Flexibility to the Process of Tip Growth

Armin Haupt,[1] Dmitry Ershov,[1,2] and Nicolas Minc[1,3,*]
[1]Institut Jacques Monod, CNRS UMR7592 and Université Paris Diderot, 15 Rue Hélène Brion, 75205 Paris Cedex 13, France
[2]Image Analysis Hub, Institut Pasteur, 25–28 Rue du Dr Roux, 75015 Paris, France
[3]Lead Contact
*Correspondence: nicolas.minc@ijm.fr
https://doi.org/10.1016/j.cub.2018.09.022

SUMMARY

Polar cell growth is a conserved morphogenetic process needed for survival, mating, and infection [1, 2]. It typically implicates the assembly and spatial stabilization of a cortical polar domain of the active form of a small GTPase of the Rho family, such as Cdc42, which promotes cytoskeleton assembly and secretion needed for local surface expansion [3–6]. In multiple physiological instances, polarity domains may switch from being spatially unstable, exhibiting a wandering behavior around the cell surface, to being stable at a fixed cellular location [7–11]. Here, we show that the rate of surface growth may be a key determinant in controlling the spatial stability of active Cdc42 domains. Reducing the growth rate of single rod-shaped fission yeast cells using chemical, genetic, and mechanical means systematically causes polar domains to detach from cell tips and oscillate around the cell surface within minutes. Conversely, an abrupt increase in growth rate improves domain stabilization. A candidate screen identifies vesicular transport along actin cables as an important module mediating this process. Similar behavior observed in distant filamentous fungi suggests that this positive feedback between growth and polarity could represent a basal property of eukaryotic polarization, promoting persistent polar growth as well as growth redirection with respect to the mechanical environment of cells.

RESULTS AND DISCUSSION

Single-Cell Manipulation of Growth Rate Impacts the Stability of GTP-Cdc42 Polarity

Polar domains of the active form of the Rho-like GTPase Cdc42 promote local growth. Studies in yeast and fungal cells have shown that polar domains can oftentimes become unstable, assembling and disassembling at successive positions around the cell surface [5, 7, 9, 11–13]. Motivated by the observation that faint and unstable domains are associated with slow surface growth [7, 9, 12], we sought to dissect the causal-effect relationships between growth and polarity, and assay in a systematic manner the impact of modulating surface growth rate on polarity stability.

Using the rod-shaped fission yeast *Schizosaccharomyces pombe* as an established model for polar growth [14], we first manipulated growth rate by reducing turgor pressure that serves as a physical driver for growth in walled cells [15]. We used a *gpd1Δ* mutant, defective in turgor adaptation, expressing the CRIB-3GFP probe to label active GTP-Cdc42, and used a defined concentration of sorbitol to reduce turgor and consequent growth rates in a reproducible manner [6, 16, 17]. In normal medium, *gpd1Δ* cells exhibited the same amount of tip-associated active Cdc42 as wild-type (WT), and no gross defect in cell shape, size, or growth (Figure S1A). Using microfluidic flow chambers [18], we rapidly rinsed cells with medium containing 0.5 M sorbitol. This caused a transient cell shrinkage, followed by a stable reduction in growth rate of ~80% within 5–10 min (Figure 1A) [6]. Strikingly, as growth rate dropped, GTP-Cdc42 domains became dimmer and more spread out, with the appearance of transient ectopic patches of activity on cell sides (Figures 1A and 1B; Video S1). Both growth and polarity changes remained stable for at least 1 hr after treatment. CRIB-3GFP polarization index (PI), computed as the ratio of membrane-associated signal at cell tips to that of the whole cell contour, decreased from a mean value of 2.02 before treatment down to 1.50 after treatment. Importantly, rinsing cells back into normal medium led to a rapid rise in growth rate and concomitant increase in CRIB PI, suggesting that this effect is reversible (Figure S1B). Similar treatment in WT cells only yielded a partial and transient reduction of both growth rate and CRIB PI (Figure S1C).

As another means to affect growth, we abruptly reduced the glucose content of the yeast medium to 0.03%. This caused WT cells to swell transiently and was followed by a marked growth rate decrease (Figure 1C; Video S1). CRIB PI also dropped following growth arrest, with cells featuring cap spreading and occasional domains forming on cell sides (Figure 1C). Finally, we exploited a global slow-growth phenotype of a *trk1Δtrk2Δ* mutant deficient in potassium import and export, which can be rescued by addition of 50 mM KCl to the medium [19]. We found that addition of KCl to these mutant cells increased their growth rate by ~30% within a few minutes and was accompanied by a significant improvement in CRIB

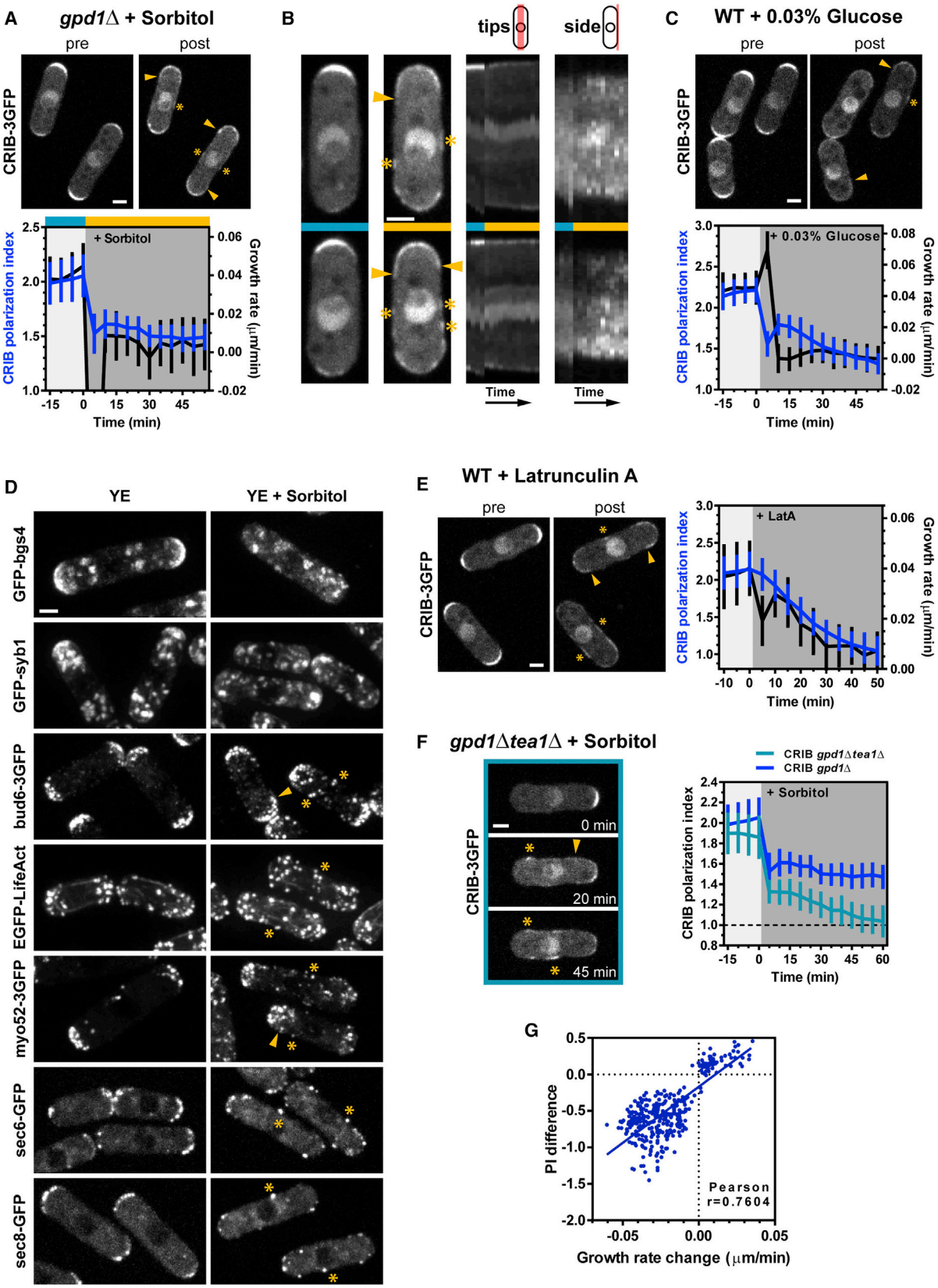

(legend on next page)

polarization (Figure S1D; Video S1). Together, these results suggest that growth may positively influence the stability of active Cdc42 polarity domains.

Influence of Growth on Other Polarity Factors

We next addressed the response of other polarisome components to turgor reduction-mediated growth arrest. Landmark factors such as microtubules and tea1-3GFP did not exhibit significant changes in their spatial distribution (Figures S1E and S1F). In contrast, polarity factors downstream of Cdc42 including the actin-associated protein bud6-3GFP, the type V myosin myo52-3GFP, and exocyst components such as sec8-GFP and sec6-GFP all showed some degree of reduced polarization with occasional domain assembly on cell sides, co-localized with CRIB (Figures 1D, S1F, and S1G).

F-actin visualized with a GFP-LifeAct probe [20] remained mostly intact, suggesting that polarity defects were not caused by some indirect stress effects on actin polymerization. However, we noted some defects in the spatial organization of F-actin structures. At a short timescale after sorbitol addition, endocytic patches exhibited a transient increase in number (Figure S1H) [21]. On longer timescales of more than 5–10 min, the actin network appeared disorganized as compared to controls, with the occurrence of cable elongation and endocytic patches at cell sides, consistent with the presence of GTP-Cdc42 there (Figures 1D and S1H).

Finally, polarized integral membrane components transported in vesicles to cell tips, such as the cell-wall synthase GFP-bgs4 and the SNARE GFP-syb1, exhibited near-complete detachment from the membrane with consequent enrichment in internal compartments (Figures 1D, S1F, S1I, and S1J). Importantly, this complete detachment was not observed for non-polar integral membrane proteins such as GFP-psy1 [22], suggesting that this response was not the result of potential pleiotropic insults on membrane shape and structure (Figures S1E and S1F). These findings suggest that growth may positively influence the stability of Cdc42-based polarity as a whole.

Although growth reduction did not grossly affect actin polymerization, its impact on polarity was somewhat reminiscent of cells treated with the actin-depolymerizing drug latrunculin A (LatA) [23]. Because LatA halts growth in yeast, we asked whether its effect on growth could account for some of its impact on polarity stability. Time-controlled LatA addition yielded a gradual decrease of the growth rate, eventually dropping to similar levels as with sorbitol treatment after 45 min (Figure 1E; Video S1). Interestingly, CRIB polarization dropped with similar kinetics, but LatA caused CRIB domains to completely detach from cell tips and to re-form on cell sides, as previously reported (Figure 1E) [23, 24].

We reasoned that F-actin could promote some of the remnant CRIB localization at cell tips in turgor-reduced cells by mediating directly or indirectly GTP-Cdc42 domain association with tip landmarks such as tea1p. To test this, we arrested growth with sorbitol in a *gpd1Δtea1Δ* double mutant. This led to near-complete depolarization, which recapitulated the effect of LatA treatment on CRIB domains in turgid cells (Figure 1F; Video S1). These results suggest that landmarks retain a fraction of active Cdc42 at cell tips upon growth arrest in an actin-dependent manner.

Finally, by computing the dependence of CRIB PI changes on growth rate variations using all aforementioned assays, we found a significant correlation ($r = 0.7604$) (Figure 1G). We conclude that growth may promote polarity stability in a dose-dependent manner.

Growth Inhibition by Physical Confinement Destabilizes Polarity

Growth in turgid cells may be influenced by external mechanical barriers such as neighboring cells, physical obstacles, or cell-encasing layers [6, 9, 13, 25]. To assay this, we designed dedicated narrow channels to confine cells laterally but allow them to grow from their ends [26, 27] (Figure 2A). WT cells growing in those channels initially proliferated with similar rates as controls outside (Figure S2A) but, as density increased, they started to hamper one another's growth. Cells reaching high levels of confinement ceased growth or grew very slowly, and adopted small triangular or rectangular shapes (Figure 2B). Remarkably, growth-arrested cells exhibited weak CRIB domains, oftentimes dynamically exploring the cell contour away from cell tips, reminiscent of turgor reduction assays (Figure 2B; Video S2). Polar components, including bud6-3GFP, LifeAct-mCherry, sec6-GFP, sec8-GFP, and GFP-bgs4, were also spatially destabilized as in turgor reduction-mediated growth arrest and exhibited dynamic changes in localization (Figures 2C, 2D, and

Figure 1. Abrupt Growth Rate Changes Alter the Localization of Cell-Polarity Factors

(A) *gpd1Δ* cells expressing CRIB-3GFP rinsed in YE medium with 0.5 M sorbitol to reduce turgor pressure and halt growth (n = 36). Top: representative cells before and after treatment. Bottom: evolution of growth rate (black) and CRIB-3GFP polarization index (PI; blue).

(B) Representative *gpd1Δ* CRIB-3GFP cells before (left) and after (right) sorbitol treatment. Right: kymographs of the same cells as in the left panels showing signal intensities of a central 1.6-μm and a lateral 0.5-μm segment over 80 min with 5-min intervals. Colors correspond to growth conditions as labeled in the graph in (A).

(C) Wild-type cells expressing CRIB-3GFP rinsed in YE medium with 0.03% glucose (n = 46). Top: representative cells before and after treatment. Bottom: evolution of growth rate (black) and CRIB-3GFP PI (blue).

(D) Subcellular localization patterns of different polarity factors in *gpd1Δ* cells in YE and after 30 min of treatment in YE + 0.5 M sorbitol.

(E) Wild-type cells expressing CRIB-3GFP treated with 50 μM latrunculin A (LatA) (n = 46). Left: representative cells before and after treatment. Right: evolution of growth rate (black) and CRIB-3GFP PI (blue).

(F) *gpd1Δ* (n = 36) and *gpd1Δtea1Δ* (n = 45) cells treated with 0.5 M sorbitol. Left: changes in CRIB-3GFP localization in *gpd1Δtea1Δ* cells. Right: evolution of PI over time for both strains.

(G) Correlation of CRIB-3GFP PI changes as a function of growth rate changes of all cells from experiments in (A), (C), (E), and (F). Pearson correlation coefficient, r = 0.7604.

In all images, arrowheads label spread caps, and asterisks mark lateral accumulations of polarity factors. Scale bars, 2 μm. Error bars represent SD. Data are from two or more independent experiments. See also Figure S1 and Video S1.

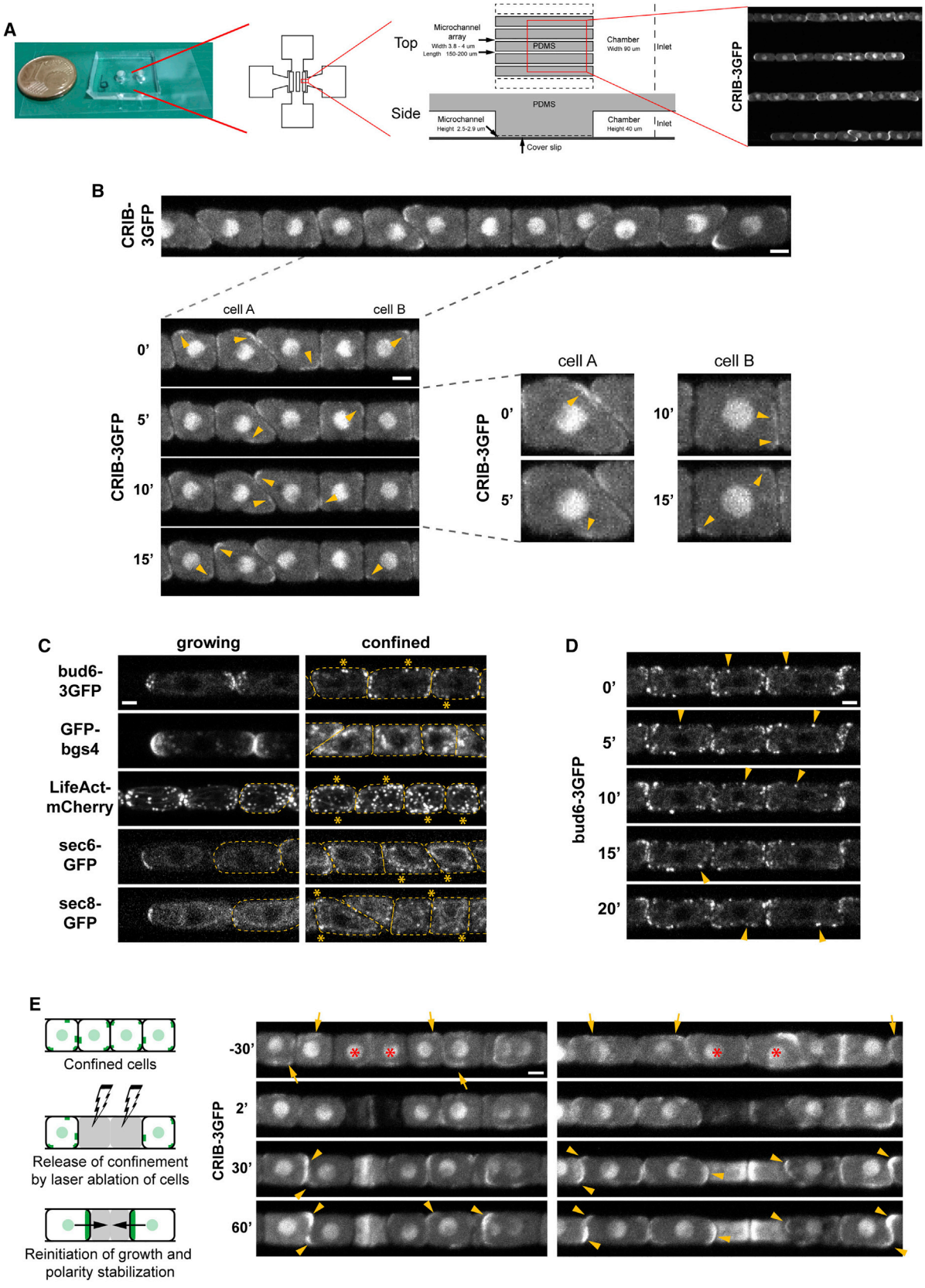

(legend on next page)

S2D). Importantly, dynamic assembly and disassembly of ectopic domains were still highly pronounced in *mal3Δ* and *tea1Δ* mutants in channels, ruling out a role for microtubule-based polarity reorganization following shape changes in CRIB domain instability (Figures S2B and S2C) [28, 29]. Thus, hampering growth by external mechanical means can yield significant destabilization of polarity domains.

Because confinement in channels is reached as a result of multiple phases of growth and division, we devised an assay to rapidly suppress confinement and assay polarity response. We started with fully confined and depolarized cells and used UV laser ablation to kill a subset of cells in the microchannel (Figure 2E; Video S3) [9]. Ablated cells deflated within seconds, freeing space for adjacent cells to grow (Figure 2E). Strikingly, ~10–20 min after ablation, neighboring cells resumed rapid growth with the concomitant formation of bright and stable CRIB-3GFP domains at growth sites. Importantly, this response was also observed in cells at a further distance from the gaps, ruling out putative effects of chemical release from ablated cells or contact-inhibition cues on polarity stability (Figure 2E). These findings demonstrate that cells can dynamically adapt their polarity behavior to different confinement states altering growth.

A Candidate Screen Identifies Suppressors and Enhancers for the Impact of Growth on Polarity Stability

To identify potential factors mediating these effects, we then designed a candidate screen using the *gpd1Δ*-sorbitol growth arrest assay (Figure 3A). We selected candidates from different classes of sensing and regulating systems, including components of the cell-wall integrity pathway, factors feeding into polarity, and a set of globally acting protein kinases and modulators that have been implicated in growth or polarity before (Figures 3B and S3A–S3D). We crossed candidate mutants into a *gpd1Δ* background expressing CRIB-3GFP or CRIB-3Citrine [24], and computed the ratio of CRIB PI after and before sorbitol addition (Figures S3A–S3D). This screen identified suppressors, in which CRIB PI after growth reduction was maintained at a higher level than *gpd1Δ* controls. Mutants in actin cable-dependent transport, such as a mutant in the formin for3 and in the myosin type V myo52, had the most pronounced suppressing effect [14]. Mutants in signaling components including the stress-related MAP kinase sty1 and in the TOR-activating Rab family GTPase ryh1 exhibited a lower, yet significant, suppression (Figures 3B–3D and S3D) [30, 31]. This screen also identified enhancers including mutants for the Cdc42 GAP rga4 and in the landmark tea1, as discussed above (Figures 1F and 3B). Because both factors have established roles in confining GTP-Cdc42 to cell tips, this result could reflect that spatial landmarks outcompete the basal destabilizing impact of growth arrest on polarity. Finally, a mutant in the endocytosis-promoting factor end4 and in the Cdc42 GEF gef1 also exhibited milder enhancing effects (Figures 3B–3D).

To test the epistatic relationships between suppressing pathways, we compared the responses of *gpd1Δfor3Δ*, *gpd1Δsty1Δ*, and *for3Δsty1Δ* with *gpd1Δ* alone (Figures 3E, 3F, and S3E). We resorted to using a *for3Δsty1Δ* mutant, because we were unable to obtain a viable *gpd1Δfor3Δsty1Δ* triple mutant, but noted that this double mutant, as in *gpd1Δ* background strains, did not adapt growth upon sorbitol treatment, due to the absence of sty1. Interestingly, in *for3Δsty1Δ* cells, we found that polarization upon growth arrest remained nearly indistinguishable from the pre-treatment state (Figures 3E and 3F). Although this analysis cannot fully rule out unknown direct effects of gpd1 on polarity stability, it indicates that actin cable-mediated transport acts independent of sty1 in this response.

Because sty1p is an established downstream target of hyperosmotic treatments and can drive active Cdc42 dispersal from cell tips when ectopically activated [24], the suppressing effects of *sty1Δ* could represent an assay-specific bias. However, the effect on polarity removal here is rather mild as compared to that reported for ectopic activation. Thus, an open possibility is that sty1 becomes partly activated as a general response to growth arrest and contributes to the detachment of GTP-Cdc42. The implication of actin-based vesicle delivery, which feeds directly into Cdc42 polarity, may be more generic, and suggests that an imbalance or mis-regulation of vesicle fluxes could serve as a core mechanism allowing cells to adapt polarity to their growth rate [5, 8]. Vesicle flows into the tip membrane may have enhanced polarity-diluting effects when surface growth is slowed down [8, 32, 33]. An alternative effect could come from defects in vesicle docking and/or fusion associated with alterations in tip membrane biochemistry or mechanics resulting from growth defects.

One interesting finding is that endocytosis appears to promote the maintenance of active Cdc42 at cell tips but is required for the detachment of the cell-wall synthase bgs4 from cell tips (Figure S1J). Accordingly, the detachment of bgs4 happens much slower, and was recently reported to depend on the cell-wall mechanical sensor wsc1 [34], which did not appear to affect active Cdc42 detachment (Figure 3B). This suggests that different mechanisms acting at various timescales may control

Figure 2. Growth Arrest through Mechanical Confinement Triggers Polarity Domain Destabilization and Wandering

(A) Large-scale picture and schematic representation of microchannel design. Three columns, each containing microchannel arrays of different length, are embedded within a large medium reservoir ("chamber") for optimal nutrient supply. PDMS, polydimethylsiloxane.

(B) Wild-type (WT) cells expressing CRIB-3GFP grown to confinement in microchannels (top). Arrowheads label transiently forming CRIB domains on the surface. Time-lapse images of confined cells (bottom left) and close-up view of two cells as labeled on the left (bottom right).

(C) WT cells expressing the indicated polarity markers grown in free-growing and fully confined regions in the same set of microchannels. Asterisks indicate ectopic accumulations of polar markers.

(D) WT cells expressing bud6-3GFP grown to full confinement in microchannels. Arrowheads label transiently forming bud6-3GFP ectopic small domains wandering on the surface.

(E) WT cells expressing CRIB-3GFP were grown in microchannels to full confinement and two cells, labeled with red asterisks, were ablated with a UV laser to free space for neighbors to grow. Arrows label initially transient or weak CRIB domains, and arrowheads depict re-forming stable CRIB domains.

Scale bars, 2 μm. See also Figure S2 and Videos S2 and S3.

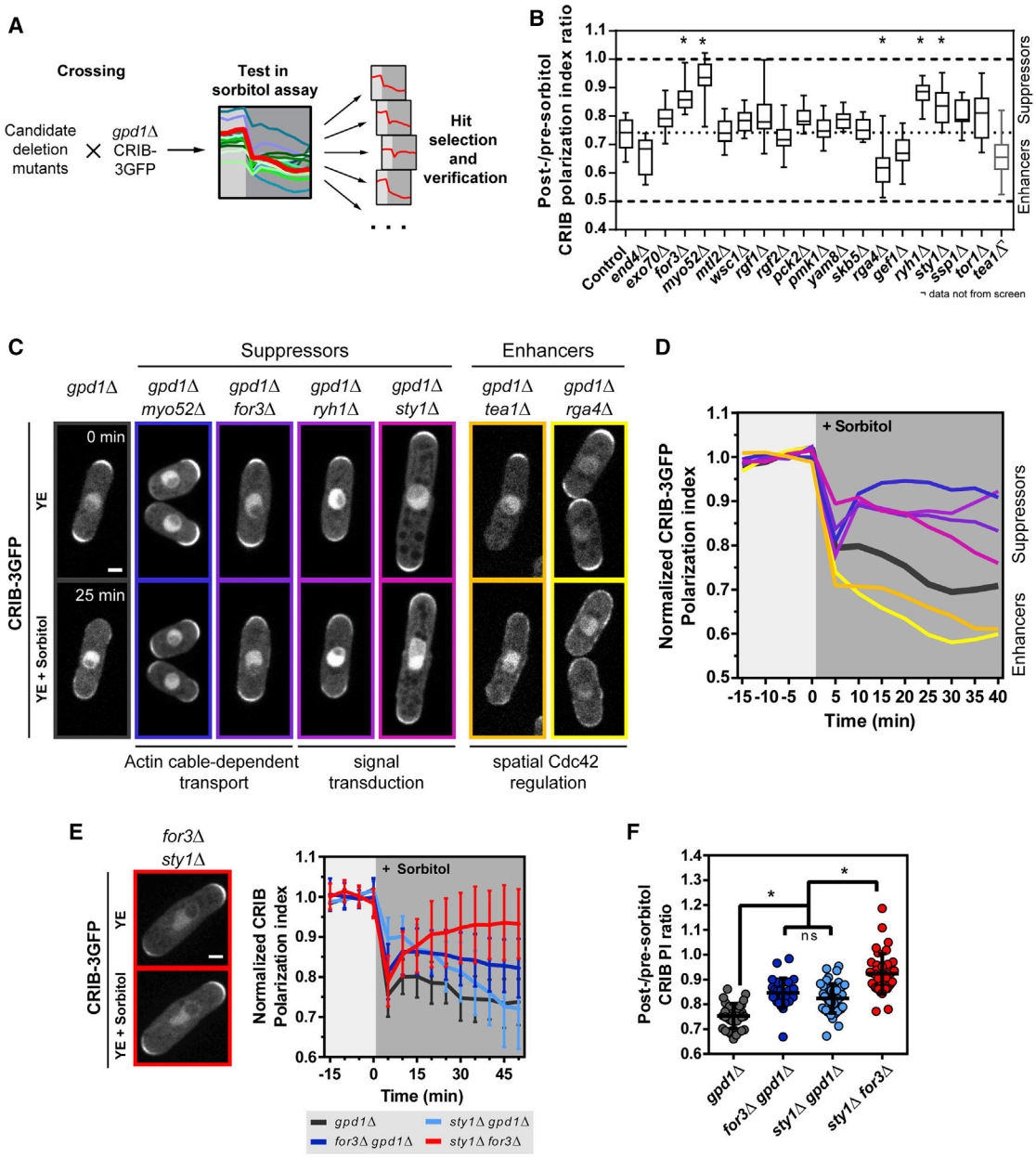

Figure 3. Candidate Genetic Screen for Modulators of Active Cdc42 Domain Destabilization upon Growth Reduction

(A) Schematic representation of the screening approach.

(B) Overview of screen results plotted as the post/pre-sorbitol ratio of the CRIB-3GFP PI. Boxplots depict the mean with 25th and 75th percentiles, and whiskers depict the full data range. Dashed lines indicate upper and lower limits of the range of values for no change or complete loss of polarization, respectively. The middle dotted line depicts values for the control. For control versus *for3Δ*, *myo52Δ*, *ryh1Δ*, *rga4Δ*, and *sty1Δ*, marked with asterisks, there was a statistically significant difference between groups as determined by one-way ANOVA ($F(19, 330) = 40.49$, $p < 0.0001$). *tea1Δ* values plotted for comparison are derived from the experiment in Figure 1F but were not included in the statistical analysis because of non-matching experimental conditions.

(C) Representative images of CRIB-3GFP response of candidates derived from the screen directly before (0 min) and 25 min after exposure to 0.5 M sorbitol.

(D) Mean response curves of CRIB-3GFP PI for hits from the screen. Colors and genotypes are matched with (C).

(E) Effect of *for3Δ* and *sty1Δ* deletions on CRIB-3GFP polarization upon treatment with 0.5 M sorbitol. Left: images showing CRIB-3GFP distribution in *for3Δsty1Δ* cells before and after sorbitol treatment. Right: CRIB-3GFP PI during sorbitol treatment (*gpd1Δ* [n = 36], *for3Δgpd1Δ* [n = 28], *sty1Δgpd1Δ* [n = 34], and *for3Δsty1Δ* [n = 39]).

(F) Comparison of post/pre-sorbitol PI ratio of CRIB-3GFP. For *gpd1Δ* versus *for3Δgpd1Δ*, *sty1Δgpd1Δ*, and *for3Δsty1Δ*, as marked by asterisks, there was a statistically significant difference between groups as determined by one-way ANOVA ($F(3, 144) = 45.112$, $p < 0.0001$; ns, not significant).

Scale bars, 2 μm. Error bars represent SD. Data, except in (B), come from two or more independent experiments. See also Figure S3 and Video S3.

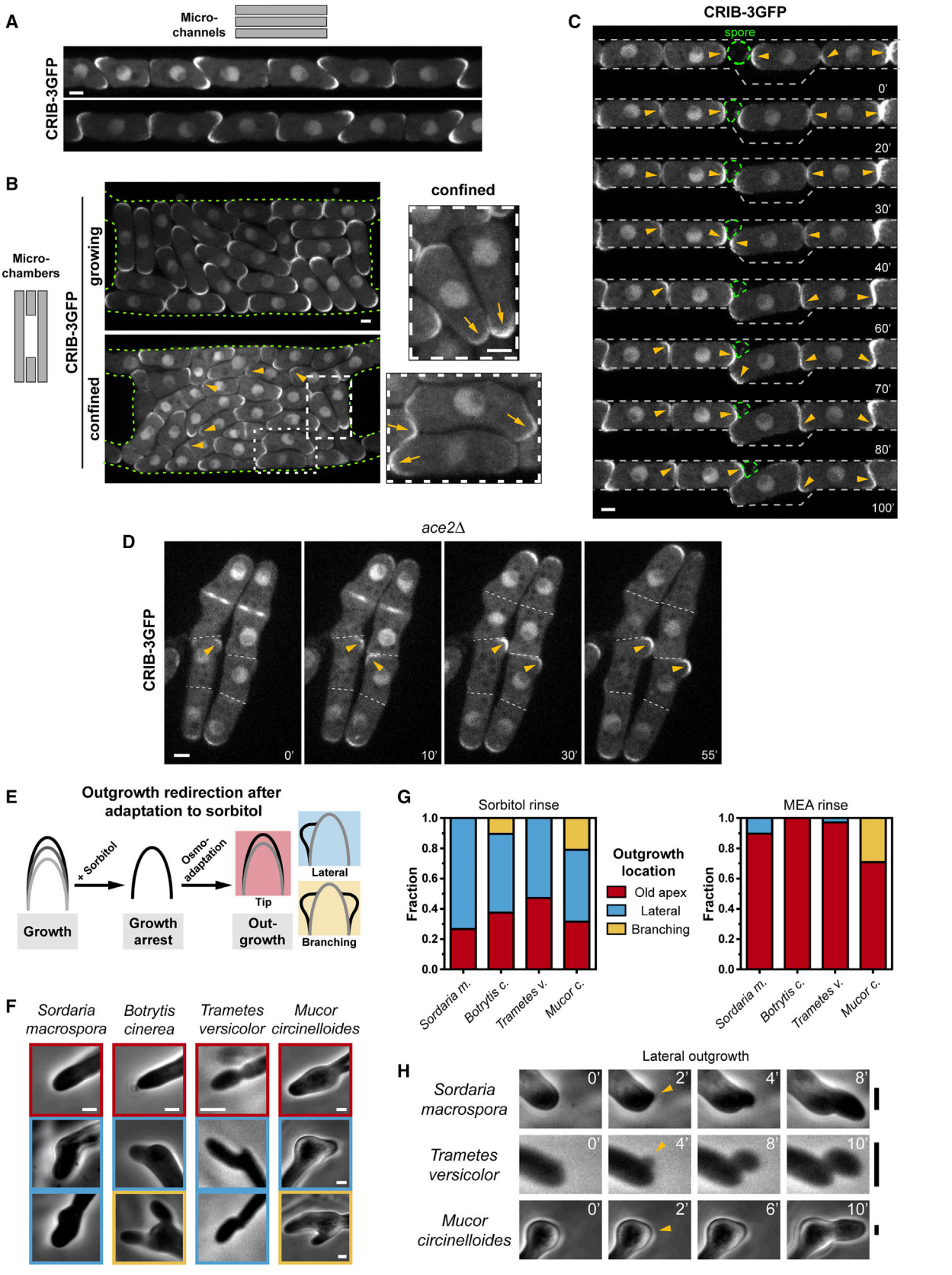

(legend on next page)

the response of polarity and growth-promoting components to growth arrest.

Feedback between Growth and Polarity as a Means to Reorient Growth around Physical Obstacles

We then asked what could be the functional relevance of a feedback between growth and polarity stability. By observing cells growing in 1D or 2D microchannels, we noted that cell tips that met end-on and were unable to displace one another systematically started to grow into available spaces by actively reorienting polar growth, yielding a high proportion of bent cells (Figures 4A and 4B). Such behavior implicated a first phase of destabilized polarity due to growth blockage by other cells, which served to locate empty spaces. This was evident from monitoring cells that grew onto each other or onto an obstacle, such as a non-germinated spore (Figures 4C and S4A; Video S4). In those instances, polarity could dynamically reorient multiple times, sometimes stabilizing at the other cell end, before causing marked shape changes, in a window as short as 20–30 min responding to newly available narrow gaps (Figure 4C, 40′).

Furthermore, we observed a similar dynamic behavior outside a microchannel using an *ace2Δ* mutant, in which cell separation is strongly impaired. This mutant bears defects in cell separation, yielding chains of 4 or more cells, with flanked middle cells that cannot grow from their tips [35]. In middle cells, CRIB-3GFP domains were weak and dynamically changed their positions and became bright and stable upon outgrowth from the side of the chain, much like WT cells in channels (Figure 4D). This behavior was never observed in front cells free to grow from their tips. We conclude that a positive feedback between growth and polarity provides cells with a functional module to dynamically reorient their growth axis toward empty spaces.

Universality of Feedback between Growth and Polarity

To test whether this effect was a conserved feature of tip-growing cells, we assayed responses in several filamentous fungus species belonging to distant branches of the fungal tree, including zygomycetes (*Mucor*), basidiomycetes (*Trametes* and *Coprinus*), and ascomycetes (*Sordaria* and *Botrytis*) (Figure S4B). We grew fungi in flow channels, rinsed them in hyperosmotic medium (0.2–0.5 M sorbitol, depending on the species), and monitored their directional response after osmo-adaptation. This treatment led to a complete cessation of hyphal growth, followed by a resumption of rapid growth after an adaptation delay (Figures 4E and S4C). Strikingly, when cell growth recommenced, hyphae grew from the sides of the apex in 50%–70% of cases, and occasionally branched (Figures 4F and 4G). This response was independent of hyphal diameter and also prominent in newly formed branches. Importantly, this altered polarized behavior was dependent on growth arrest, as flowing in medium did not affect hyphal polarization (Figures 4G and S4D). In some species, such as *Botrytis* or *Mucor*, lateral branch formation following growth arrest was preceded by a brief period of isotropic growth, indicative of initial polarity dispersal before local stabilization (Figures 4F and 4H). One species, *Coprinus cinereus*, formed lateral branches following growth arrest and recovery, mainly at large distances from the apex (30–60 μm), plausibly reflecting inherent mechanisms that suppress tip-proximal branching (Figure S4E). Although this growth redirection behavior created some sharp shape changes at the hyphal tip, we noted that, on a global scale, hyphae continued their mean growth direction away from the bulk of the colony, most likely guided by some tropisms [1]. These results support a plausible universality for a feedback between growth and polarity relevant to most fungal species.

In sum, we propose a dynamic feedback linking growth and polarity stability: when polarity domains form at the surface, they become stable if growth occurs at a normal or high rate and disassemble if growth is hindered mechanically or chemically (Figure S4F). This feedback may account for persistent polar growth typical of yeast and fungal cells independent of guiding cues or spatial landmarks [9, 36, 37]. Accordingly, this mechanism appears more prominent in the absence of internal landmarks provided by the tea1 system in fission yeast, and may compete with global guiding cues in fungal hyphae (Figures 1F and 4F). This feedback could also synchronize, or phase lock, Rho GTPase oscillations and pulsatile growth typical of many tip-growing cells [38, 39]. One important realization, however, is that growth rates in yeast and other walled cells remain bounded. Thus, in addition to positive feedback, limitation systems either based upon the availability of polarity or growth factors or encoded in the mechanics of the surface must exist to buffer growth [34].

In addition to conferring spatial persistency to polar growth, this mechanism also provides flexibility, by allowing cells to reorient growth in directions that are mechanically favorable. Many tip-growing cells, including fungal hyphae and plant roots, exhibit thigmotropisms and can redirect their growth axis in

Figure 4. Universal Feedback between Growth and Polarity as a Means to Reorient Polar Growth Axis

(A) WT cells expressing CRIB-3GFP grown in microchannels and observed at a stage of early confinement.

(B) WT cells expressing CRIB-3GFP grown in 2D microchambers and observed at a stage of low (left top) and high (left bottom) confinement. Insets: magnifications of cells in high confinement (right). Arrowheads point to examples of weak CRIB-3GFP domains, and arrows label irregularly shaped cell tips.

(C) WT cells expressing CRIB-3GFP growing from the two opposite ends of a channel and reorienting polarity and growth upon contact. Arrowheads indicate CRIB domains that change position. The green dashed circles depict the outline of a dormant spore acting as a rigid obstacle.

(D) *ace2Δ* cells expressing CRIB-3GFP grown on YE agar. As a consequence of delayed cell separation, some cells are flanked by two sister cells and finally outgrow from the sides. Arrowheads label initially transient or weak CRIB domains that become stabilized and intense as cells outgrow.

(E) Assaying outgrowth direction of filamentous fungi after recovery from sorbitol-induced growth arrest.

(F) Representative hyphal shapes following growth recovery after sorbitol treatment in various fungal species. Colors are related to response classification in (G).

(G) Quantification of the different hyphal phenotypes reflecting a transient alteration of polarization behavior following growth arrest and recovery. For sorbitol rinse: *Sordaria macrospora*, n = 30; *Botrytis cinerea*, n = 39; *Trametes versicolor*, n = 36; *Mucor circinelloides*, n = 19. For malt extract agar (MEA) rinse: *S. macrospora*, n = 29; *B. cinerea*, n = 26; *T. versicolor*, n = 34; *M. circinelloides*, n = 24.

(H) Time-lapse images of lateral outgrowth at the hyphal tips in different species. Arrowheads point at emerging polar growing tips.

Scale bars, 2 μm (A–D) and 4 μm (F and H). See also Figure S4 and Video S4.

response to mechanical stimuli, when navigating in tissues or in soil, for instance [40]. The feedback we document here could in principle serve as an inherited trait promoting such behavior even in a simple yeast cell.

Although growth is the prominent driver of cell-surface deformation in fungal cells, other eukaryotic cells that migrate or are submitted to tissue forces may also employ similar conceptual feedbacks to support the stability of polarity machineries with respect to their rates of surface deformation. Accordingly, recent work has suggested near-universal correlations between directional persistence and locomotion speed in migrating cells [41]. Cell-surface deformations, which originate from patterns of tissue stress, may also promote cell polarization along specific tissue axes in animal [42] and plant tissues [43]. Further work addressing the interconnections between dynamic shape changes and directional behaviors will illuminate mechanisms of eukaryotic morphogenesis.

STAR★METHODS

Detailed methods are provided in the online version of this paper and include the following:

- KEY RESOURCES TABLE
- CONTACT FOR REAGENT AND RESOURCE SHARING
- EXPERIMENTAL MODEL AND SUBJECT DETAILS
  - Yeast strains, genetic methods, and media
  - Filamentous fungi species, media and growth
  - Pharmacological inhibition
- METHOD DETAILS
  - Flow channels
  - Microchannels for confined growth assays
  - Microscopy
- QUANTIFICATION AND STATISTICAL ANALYSIS
  - Image analysis
  - Extraction of single cell data
  - Statistical analysis

SUPPLEMENTAL INFORMATION

Supplemental Information includes four figures, one table, and four videos and can be found with this article online at https://doi.org/10.1016/j.cub.2018.09.022.

ACKNOWLEDGMENTS

The authors acknowledge M. Balasubramanian, Q. Chen, M. Edamatsu, S. Martin, P. Perez, Y. Sanchez, K. Sawin, and F. Leclerc for sharing strains and material. This work was supported by the CNRS and grants from the Mairie de Paris "Emergence" program and the European Research Council (CoG Forcaster 647073).

AUTHOR CONTRIBUTIONS

A.H. performed the experiments and analyzed the data. D.E. developed image analysis scripts. A.H. and N.M. designed the research and wrote the manuscript.

DECLARATION OF INTERESTS

The authors declare no competing interests.

Received: April 26, 2018
Revised: July 24, 2018
Accepted: September 11, 2018
Published: October 11, 2018

REFERENCES

1. Brand, A., and Gow, N.A. (2009). Mechanisms of hypha orientation of fungi. Curr. Opin. Microbiol. *12*, 350–357.
2. Merlini, L., Dudin, O., and Martin, S.G. (2013). Mate and fuse: how yeast cells do it. Open Biol. *3*, 130008.
3. Li, R., and Gundersen, G.G. (2008). Beyond polymer polarity: how the cytoskeleton builds a polarized cell. Nat. Rev. Mol. Cell Biol. *9*, 860–873.
4. Johnson, J.M., Jin, M., and Lew, D.J. (2011). Symmetry breaking and the establishment of cell polarity in budding yeast. Curr. Opin. Genet. Dev. *21*, 740–746.
5. Martin, S.G. (2015). Spontaneous cell polarization: feedback control of Cdc42 GTPase breaks cellular symmetry. BioEssays *37*, 1193–1201.
6. Minc, N., Boudaoud, A., and Chang, F. (2009). Mechanical forces of fission yeast growth. Curr. Biol. *19*, 1096–1101.
7. Bendezú, F.O., and Martin, S.G. (2013). Cdc42 explores the cell periphery for mate selection in fission yeast. Curr. Biol. *23*, 42–47.
8. Bonazzi, D., Haupt, A., Tanimoto, H., Delacour, D., Salort, D., and Minc, N. (2015). Actin-based transport adapts polarity domain size to local cellular curvature. Curr. Biol. *25*, 2677–2683.
9. Bonazzi, D., Julien, J.D., Romao, M., Seddiki, R., Piel, M., Boudaoud, A., and Minc, N. (2014). Symmetry breaking in spore germination relies on an interplay between polar cap stability and spore wall mechanics. Dev. Cell *28*, 534–546.
10. Merlini, L., Khalili, B., Bendezú, F.O., Hurwitz, D., Vincenzetti, V., Vavylonis, D., and Martin, S.G. (2016). Local pheromone release from dynamic polarity sites underlies cell-cell pairing during yeast mating. Curr. Biol. *26*, 1117–1125.
11. Dyer, J.M., Savage, N.S., Jin, M., Zyla, T.R., Elston, T.C., and Lew, D.J. (2013). Tracking shallow chemical gradients by actin-driven wandering of the polarization site. Curr. Biol. *23*, 32–41.
12. Howell, A.S., Jin, M., Wu, C.F., Zyla, T.R., Elston, T.C., and Lew, D.J. (2012). Negative feedback enhances robustness in the yeast polarity establishment circuit. Cell *149*, 322–333.
13. Thomson, D.D., Wehmeier, S., Byfield, F.J., Janmey, P.A., Caballero-Lima, D., Crossley, A., and Brand, A.C. (2015). Contact-induced apical asymmetry drives the thigmotropic responses of *Candida albicans* hyphae. Cell. Microbiol. *17*, 342–354.
14. Chang, F., and Martin, S.G. (2009). Shaping fission yeast with microtubules. Cold Spring Harb. Perspect. Biol. *1*, a001347.
15. Davì, V., and Minc, N. (2015). Mechanics and morphogenesis of fission yeast cells. Curr. Opin. Microbiol. *28*, 36–45.
16. Ohmiya, R., Yamada, H., Nakashima, K., Aiba, H., and Mizuno, T. (1995). Osmoregulation of fission yeast: cloning of two distinct genes encoding glycerol-3-phosphate dehydrogenase, one of which is responsible for osmotolerance for growth. Mol. Microbiol. *18*, 963–973.
17. Tatebe, H., Nakano, K., Maximo, R., and Shiozaki, K. (2008). Pom1 DYRK regulates localization of the Rga4 GAP to ensure bipolar activation of Cdc42 in fission yeast. Curr. Biol. *18*, 322–330.
18. Charvin, G., Cross, F.R., and Siggia, E.D. (2008). A microfluidic device for temporally controlled gene expression and long-term fluorescent imaging in unperturbed dividing yeast cells. PLoS ONE *3*, e1468.
19. Calero, F., Gómez, N., Ariño, J., and Ramos, J. (2000). Trk1 and Trk2 define the major K(+) transport system in fission yeast. J. Bacteriol. *182*, 394–399.
20. Courtemanche, N., Pollard, T.D., and Chen, Q. (2016). Avoiding artefacts when counting polymerized actin in live cells with LifeAct fused to fluorescent proteins. Nat. Cell Biol. *18*, 676–683.

21. Basu, R., Munteanu, E.L., and Chang, F. (2014). Role of turgor pressure in endocytosis in fission yeast. Mol. Biol. Cell *25*, 679–687.
22. Nakamura, T., Nakamura-Kubo, M., Hirata, A., and Shimoda, C. (2001). The *Schizosaccharomyces pombe* spo3+ gene is required for assembly of the forespore membrane and genetically interacts with psy1(+)-encoding syntaxin-like protein. Mol. Biol. Cell *12*, 3955–3972.
23. Bendezú, F.O., and Martin, S.G. (2011). Actin cables and the exocyst form two independent morphogenesis pathways in the fission yeast. Mol. Biol. Cell *22*, 44–53.
24. Mutavchiev, D.R., Leda, M., and Sawin, K.E. (2016). Remodeling of the fission yeast Cdc42 cell-polarity module via the Sty1 p38 stress-activated protein kinase pathway. Curr. Biol. *26*, 2921–2928.
25. Sampathkumar, A., Yan, A., Krupinski, P., and Meyerowitz, E.M. (2014). Physical forces regulate plant development and morphogenesis. Curr. Biol. *24*, R475–R483.
26. Goulev, Y., Morlot, S., Matifas, A., Huang, B., Molin, M., Toledano, M.B., and Charvin, G. (2017). Nonlinear feedback drives homeostatic plasticity in H_2O_2 stress response. eLife *6*, e23971.
27. Zegman, Y., Bonazzi, D., and Minc, N. (2015). Measurement and manipulation of cell size parameters in fission yeast. Methods Cell Biol. *125*, 423–436.
28. Minc, N., Bratman, S.V., Basu, R., and Chang, F. (2009). Establishing new sites of polarization by microtubules. Curr. Biol. *19*, 83–94.
29. Terenna, C.R., Makushok, T., Velve-Casquillas, G., Baigl, D., Chen, Y., Bornens, M., Paoletti, A., Piel, M., and Tran, P.T. (2008). Physical mechanisms redirecting cell polarity and cell shape in fission yeast. Curr. Biol. *18*, 1748–1753.
30. Millar, J.B., Buck, V., and Wilkinson, M.G. (1995). Pyp1 and Pyp2 PTPases dephosphorylate an osmosensing MAP kinase controlling cell size at division in fission yeast. Genes Dev. *9*, 2117–2130.
31. Tatebe, H., Morigasaki, S., Murayama, S., Zeng, C.T., and Shiozaki, K. (2010). Rab-family GTPase regulates TOR complex 2 signaling in fission yeast. Curr. Biol. *20*, 1975–1982.
32. Savage, N.S., Layton, A.T., and Lew, D.J. (2012). Mechanistic mathematical model of polarity in yeast. Mol. Biol. Cell *23*, 1998–2013.
33. Tay, Y.D., Leda, M., Spanos, C., Rappsilber, J., Goryachev, A., and Sawin, K. (2018). Fission yeast NDR/LATS kinase Orb6 regulates exocytosis via phosphorylation of exocyst complex. bioRxiv. https://doi.org/10.1101/291468.
34. Davì, V., Tanimoto, H., Ershov, D., Haupt, A., De Belly, H., Le Borgne, R., Couturier, E., Boudaoud, A., and Minc, N. (2018). Mechanosensation dynamically coordinates polar growth and cell wall assembly to promote cell survival. Dev. Cell *45*, 170–182.e7.
35. Dekker, N., Speijer, D., Grün, C.H., van den Berg, M., de Haan, A., and Hochstenbach, F. (2004). Role of the alpha-glucanase Agn1p in fission-yeast cell separation. Mol. Biol. Cell *15*, 3903–3914.
36. Kelly, F.D., and Nurse, P. (2011). De novo growth zone formation from fission yeast spheroplasts. PLoS ONE *6*, e27977.
37. Sawin, K.E., and Snaith, H.A. (2004). Role of microtubules and tea1p in establishment and maintenance of fission yeast cell polarity. J. Cell Sci. *117*, 689–700.
38. Das, M., Drake, T., Wiley, D.J., Buchwald, P., Vavylonis, D., and Verde, F. (2012). Oscillatory dynamics of Cdc42 GTPase in the control of polarized growth. Science *337*, 239–243.
39. Hwang, J.U., Gu, Y., Lee, Y.J., and Yang, Z. (2005). Oscillatory ROP GTPase activation leads the oscillatory polarized growth of pollen tubes. Mol. Biol. Cell *16*, 5385–5399.
40. Jaffe, M.J., Leopold, A.C., and Staples, R.C. (2002). Thigmo responses in plants and fungi. Am. J. Bot. *89*, 375–382.
41. Maiuri, P., Rupprecht, J.F., Wieser, S., Ruprecht, V., Bénichou, O., Carpi, N., Coppey, M., De Beco, S., Gov, N., Heisenberg, C.P., et al. (2015). Actin flows mediate a universal coupling between cell speed and cell persistence. Cell *161*, 374–386.
42. Aw, W.Y., Heck, B.W., Joyce, B., and Devenport, D. (2016). Transient tissue-scale deformation coordinates alignment of planar cell polarity junctions in the mammalian skin. Curr. Biol. *26*, 2090–2100.
43. Nakayama, N., Smith, R.S., Mandel, T., Robinson, S., Kimura, S., Boudaoud, A., and Kuhlemeier, C. (2012). Mechanical regulation of auxin-mediated growth. Curr. Biol. *22*, 1468–1476.
44. Sato, M., Dhut, S., and Toda, T. (2005). New drug-resistant cassettes for gene disruption and epitope tagging in *Schizosaccharomyces pombe*. Yeast *22*, 583–591.
45. Fehrmann, S., Paoletti, C., Goulev, Y., Ungureanu, A., Aguilaniu, H., and Charvin, G. (2013). Aging yeast cells undergo a sharp entry into senescence unrelated to the loss of mitochondrial membrane potential. Cell Rep. *5*, 1589–1599.
46. Bendezú, F.O., Vincenzetti, V., Vavylonis, D., Wyss, R., Vogel, H., and Martin, S.G. (2015). Spontaneous Cdc42 polarization independent of GDI-mediated extraction and actin-based trafficking. PLoS Biol. *13*, e1002097.

STAR★METHODS

KEY RESOURCES TABLE

REAGENT or RESOURCE	SOURCE	IDENTIFIER
Chemicals, Peptides, and Recombinant Proteins		
LatrunculinA	Sigma-Aldrich	Cat# L5163
Gs-IB$_4$ -Alexafluor647	ThermoFisher	Cat# I32450
CK666	Sigma-Aldrich	Cat# L0006
Percoll	Sigma-Aldrich	Cat# P1644
PDMS kit (Sylgard 184)	Dow Corning	Cat# DC184
Experimental Models: Organisms/Strains		
S. pombe and filamentous fungi strains, see Table S1	N/A	N/A
Oligonucleotides		
Primer: Resistance marker switching forward: CGGATCCCCGGGTTAATTAAGGCG	[44]	MD1
Primer: Resistance marker switching reverse: GAATTCGAGCTCGTTTAAACACTGG ATGGCGGCGTTAGTATCG	[44]	MD2
Recombinant DNA		
Vector: pCR2.1-nat	[44]	NEG772014MC

CONTACT FOR REAGENT AND RESOURCE SHARING

Further information and requests for resources and reagents should be directed to and will be fulfilled by the lead contact, Nicolas Minc (nicolas.minc@ijm.fr).

EXPERIMENTAL MODEL AND SUBJECT DETAILS

Yeast strains, genetic methods, and media

Standard methods for *S. pombe* media and genetic manipulations were used (http://www-bcf.usc.edu/~forsburg; http://www.biotwiki.org/foswiki/bin/view/Pombe/NurseLabManual). Strains used in this study are listed in the Key Resources Table. Marker switching from Kan to Nat was achieved by amplifying the NatMX cassette from a pCR2.1-nat vector with primers MD1 and MD2 and transforming it into KanMX cassette-bearing strains. Positive clones were selected on YE5S + 50 μg/mL Nat plates and tested for functional and visual phenotypes [44]. For all experiments, liquid cultures were grown in YE5S (containing 3% glucose) overnight at 25°C. For experiments in flow channels, cells were pre-stained with 10 μg/mL Alexa647-labeled isolectin GS-IB4 from *Griffonia simplicifolia* (Thermo Fisher Scientific, Waltham, Massachusetts, USA) and growth medium contained a constant Lectin supply of 5 μg/mL. The lectin signal labeled the cell contour and was used for cell segmentation during image analysis.

Filamentous fungi species, media and growth

Strains: *Botrytis cinerea*, *Sordaria macrospora*, *Coprinus cinereus*, *Trametes versicolor* and *Mucor circinelloides*. All strains were grown on malt extract agar (MEA) medium (2% malt, 0.1% peptone, 2% glucose) either as liquid or plates with 2% agar. To grow hyphal mycelia, spores were prepared by lysing hyphae from a fully-grown MEA plate with glass beads and a FastPrep device (MP Biomedicals, Santa Ana, California, USA). Crude spore preparations were used to inoculate 20 mL MEA cultures and these were grown over night at 25°C. Emerging mycelia from these cultures were placed in PDMS flow channels under a dialysis membrane for microscopy.

Pharmacological inhibition

Latrunculin A (Sigma-Aldrich, St. Louis, Missouri, USA) was used at a final concentration of 50 μM from a 200x stock in DMSO (Euromedex, Souffelweyersheim, France). CK666 (Sigma-Aldrich) was used at a final concentration of 100 μM from a 500x stock in DMSO. DMSO amounts in control experiments were adjusted correspondingly for each drug.

METHOD DETAILS

Flow channels

We used two kinds of flow channels depending on the type of experiment. For drug treatments we used a simple glass channel built from one 24x50 mm (VWR, Radnor, Pennsylvania, USA) and a 22x22 mm (Thermo Fisher Scientific) coverslip spaced by ~250 μm, using double-sided adhesive tape. To make cells adhere to the glass surface, the flow channel was pre-coated with 1 mg/mL poly-L-lysine (Sigma-Aldrich) and 0.1 mg/mg isolectin GS-IB4 from *Griffonia simplicifolia*, (Thermo Fisher Scientific).

In the second type of flow channels, cells were placed beneath a single layer of dialysis membrane and covered with a polydimethylsiloxane (PDMS) channel, allowing for exchange of the medium [18].

Microchannels for confined growth assays

Design and fabrication

The general design of microchannels to confine fission yeast cells is shown in Figure 2A. Those channels were optimized to ensure a near unlimited nutrient supply, and implicated a 2-step soft-lithography microfabrication technique [45]. A first thin layer of ~2.5 μm in height was first fabricated using SU8 photoresists, and subsequent UV illumination through a Quartz mask. Subsequently, a second layer of ~40μm in height of SU8 photoresists, was spread on top of the first layer, and exposed with UV through a Quartz mask, aligned with the first design using a Mask Aligner. PolyDimethylSiloxane (PDMS, Sylgard 184 from Dow Corning, Midland, Michigan, USA) replica were prepared using a 10:1 ratio of PDMS:curing agent.

Microchannel assembly

PDMS channels were covalently mounted onto 24x50 mm coverslips (VWR) [27]. To this aim, coverslips were cleaned with Acetone, Isopropanol and ddH_2O. For covalent binding, both channel and coverslip were then plasma treated for 1 min, mounted and baked at 65°C for ≥1 hr.

Cell loading and growing

Cells were loaded into channels as spores, which then germinated and proliferated as vegetative cells, crowding the channels [27]. Spores were obtained from *h90* strains sporulated on ME/3% agarose (Formedium, Hunstanton, UK)/(Sigma-Aldrich) plates at 25°C for 2-3 days. Mating mixtures were digested in 1/200 Glusulase (PerkinElmer, Waltham, Massachusetts, USA) at room temperature overnight, to eliminate vegetative cells. Digests were cleared of debris by adding four volumes of Percoll (Sigma-Aldrich), followed by a centrifugation at 600 rcf. for 3min and supernatant removal. Spores were washed once with five volumes of YE5S and subsequently re-suspended in YE5S medium [46]. Channels were first filled with YE5S and subsequently a high density spore solution was pushed into channels with a syringe, usually yielding 1-6 spores per channel. Excess spores were rinsed out. Filled channels were incubated for 18-24 hr in a humidified Petri dish at 25 or 30°C, depending on global spore density after seeding. The next morning, channels were rinsed with fresh media at least 1 hr before live-imaging. All data presented in Figures 2, 4, S2, and S4, corresponding to cells grown in channels were reproduced at least 2 times.

Microscopy

For immediate imaging, 1.8 μL of fresh, concentrated cells were placed between a glass slide and coverslip and imaged within 20 min. For experiments with dynamic exchange of growth media / drug addition, cells were placed in different types of flow channels. Microchannels were directly imaged.

All fission yeast imaging was carried out at room temperature (22–25°C) with an inverted spinning-disk confocal microscope equipped with a motorized stage and automatic focus (Ti-Eclipse, Nikon, Minato, Tokyo, Japan), a Yokogawa CSUX1FW spinning unit, and an EM-CCD camera (ImagEM-1K, Hamamatsu Photonics, Japan). Images were acquired with a 100 × oil-immersion objective (CFI Plan Apo DM 100x/1.4 NA, Nikon). For laser ablation in microchannels we used an iLas2 module (Roper Scientific) with a 355 nm laser and acquired images with a 60x oil-immersion objective (CFI Apochromat 60x Oil λS, 1.4 NA, Nikon) in combination with a 2.5x magnifying lens. The microscope was operated with Metamorph software (Molecular Devices).

Presented images represent single confocal slices or specific z stacks: Figures 1A, 1E, 1F, 3C, and 3E: Single-plane confocal images. Figure 1D: Maximum intensity projections of 19 z-slices spaced by 0.25 μm, except for sec8-GFP which is a projection of 3 slices spaced by 0.5 μm. Figure 2B: Maximum intensity projections from 5 z-slices spaced by 0.6 μm. Figure 2C: Maximum intensity projections from 5 (bud6-3GFP, GFP-bgs4) or 3 (sec6-GFP, sec8-GFP) z-slices spaced by 0.6 μm, and from 14 slices with 0.3 μm spacing for LifeAct-mcherry. Figure 2D: Maximum intensity projections from 3 z-slices spaced by 0.6 μm. 2E: Maximum intensity projections from 11 z-slices spaced by 0.4 μm. Figure 4A: Maximum intensity projections from 7 z-slices spaced by 0.5 μm. Figure 4B: Maximum intensity projections from 5 z-slices spaced by 0.5 μm. Figure 4C: Maximum intensity projections from 5 z-slices spaced by 0.6 μm. Figure 4D: Maximum intensity projections from 3 z-slices spaced by 0.2 μm. All data presented in Figures 1, 2C–2F, S1, and S3E are from two or more independent experiments, with quantified cells selected randomly in the field. Data for the screen presented in Figures 2B and S3A–S3D were performed only once, with quantified cells selected randomly in the field. For all experiments, there was no blinding method applied, and the number of cells analyzed and quantified are indicated in corresponding figure legends.

Filamentous fungi imaging was carried out with an inverted epifluorescence microscope (Ti-Eclipse, Nikon) combined with a CMOS camera (Hamamatsu). Hyphae were filmed with a 40x dry objective (CFI Plan Fluor DLL 40X/0.75 NA, Nikon) and a 1.5x magnifier. The microscope was operated with Micro-Manager (Open Imaging). Data presented in Figures 4 and S4 are from two or more independent experiments, with quantified cells selected randomly in the field. There was no blinding method applied, and the numbers of cells analyzed are indicated in corresponding figure legends.

Inclusion and exclusion criteria of any data or subjects

The slow growth phenotype of *gpd1Δ* strains in hyperosmotic conditions was used as an inclusion criterion for this assay. This phenotype is subject to strong adaptive pressure, even when strains are grown on normal YE5S plates, leading to occasional

WT-like responses in hyperosmotic conditions. Experiments, in which *gpd1Δ* cells recovered their growth rate in 0.5 M sorbitol, were excluded after initial inspection, prior to quantitative analysis. We did not exclude individual cells that showed adapted behavior in an otherwise slow-growing population.

QUANTIFICATION AND STATISTICAL ANALYSIS

Image analysis

To analyze changes in growth rates and localization of polar factors following growth perturbations, we developed dedicated MATLAB scripts [34]. We first segmented cells using the signal from the lectin-labeled cell wall. To this aim, we first smoothed the image with median and Gaussian filters and detected cell edges using the Laplacian of the Gaussian filter. The resultant binary image was then filtered to remove small segments. Given that the signal of the labeled cell wall has a finite thickness, we detected the inner and the outer border of this signal. All spaces in this image were then filled in white except for the spaces between the inner and outer border of the wall, yielding a black band representing the cell wall. Using the watershed algorithm, we finally extracted the whole-cell contour defined as the middle of this band. To compute cell length, we fitted the long axis of the segmented cell with a polynomial of degree 3. This fit was then used to define a ''cell spine'' and its length was calculated and used as a measurement for cell length.

The whole-cell contour could then be manipulated using morphological and logical operations to obtain a set of arbitrary regions (tips, membrane, cytoplasm, etc.). The tip regions are for instance shaped as a cut off from the whole-cell mask perpendicular to the cell spine at specific distances along the spine. A segment outside of the cell can be shaped to compute the background.

Fluorescent signals of interest were then extracted from fluorescent images by using a mask based on corresponding sub-regions and are background corrected. PI was computed by normalizing the background-corrected tip signal with the background-corrected plasma membrane signal:

$$PI = \frac{I_{tip\ raw} - I_{bg}}{I_{plasma\ membrane\ raw} - I_{bg}}$$

Additional image analysis and processing for Figures was done in ImageJ (National Institutes of Health).

Extraction of single cell data

Because of marked rapid changes in cell shape (shrinkage or swelling) upon sorbitol or other treatments, PI and growth rate quantification for single cells was done as an average of data from −15 to 0 min ('pre') and from +10 min to 40 min ('post') relative to treatment, omitting data corresponding to these rapid responses. This calculation was used for the screen results (Figures 3B, 3F, S3C, and S3D). Data to compute Figure 1G were extracted in the same manner from experiments in Figures 1A, 1C, 1E, 1F, and S1D. Data post-treatment from 1E was split into two phases of slowing growth (+10 to +30 min in LatA) and no growth (+35 to +50 min in LatA). To compute the changes in PI or growth rate the difference between pre- and post-treatment values (e.g., $diff_{PI} = PI_{post} - PI_{pre}$) was calculated.

Statistical analysis

Statistical and correlation analyses were carried out using Prism 6 software (GraphPad Software, La Jolla, CA). To compute significance throughout this work, we used, one-way analysis of variance (ANOVA) followed by Dunnett multiple comparisons test or two-tailed, unpaired t test. Statistically significant difference between groups are $^*p < 0.0001$. No other particular tests were applied to determine if data distributions met the assumptions of these statistical approaches. Linear correlation was analyzed by computing the Pearson correlation coefficient.